Chapter 3

Time Averaged Simulation Parameters for Different Configurations

In this chapter, we present and discuss time-averaged turbulence parameters based on time and Fourier-domain analyses. In particular, we stress how the different configurations influence such parameters. All data analyzed in this chapter are obtained from velocity records sampled at a frequency of 4000Hz over a period of 180 seconds. The velocity measurements were taken at the height of 7.92cm, which corresponds to the height of the model. The parameters that will be discussed include mean flow Reynolds number, longitudinal mean velocity, variance, turbulence intensity, integral length scale, small scale turbulence and spectra of velocity components.

3.1 Mean Flow Reynolds Number

Simulating mean flow Reynolds number is impossible at scale ratios of 1:50 on 1:100. The full scale Reynolds could be as high as 1.5×10^7. For a 1:50 scaled model, the mean flow in model studies should be 50 times faster to satisfy Reynolds number similarity, which is not feasible. In the experiments conducted for this work, the wind tunnel speed control was set at 800 for each configuration which corresponds to a free stream speed of approximately 12 m/s. Variations of the mean velocity in the wind tunnel for constant fan

Table 3.1: Statistic quantities for eight configurations: Z=7.92cm, fan-speed=800, Var.---variance, Int.---turbulence intensity, I-length---integral length scale, S-scale---small scales$\times 10^6$

Conf.#	Ds-file	Mean (m/s)	Comp.	Var. (m^2/s^2)	I-length (m)	S-scale	Int.
Conf.#1	DsX	12.017	U	0.843	0.336	7.2	0.076
			V	0.276	0.012		0.044
Conf.#2	DsX	10.412	U	1.884	0.764	10.5	0.132
			V	1.439	0.476		0.115
Conf.#3	DsX	9.413	U	2.409	0.487	38.6	0.165
			V	2.052	0.336		0.152
Conf.#4	DsX	8.713	U	2.448	0.696	28.6	0.180
			V	1.327	0.357		0.132
Conf.#5	DsX	8.232	U	2.202	0.593	64.0	0.180
			V	1.543	0.354		0.151
Conf.#6	DsXI	9.627	U	2.237	0.525	20.5	0.155
			V	1.047	0.228		0.106
Conf.#7	DsXI	7.643	U	1.488	0.253	54.6	0.160
			V	1.221	0.054		0.145
Conf.#8	DsXI	8.055	U	2.392	0.337	47.3	0.192
			V	1.809	0.240		0.167

speed are given in table 3.1. The results show a trend whereby increased roughness size results in smaller mean velocities. The mean of u-component in the bare tunnel is about 12m/s. As big spires are added (configuration #2), this value is reduced by about 10%.

The addition of small spires as in configuration #3 causes more reduction in the mean flow. In a similar manner, the addition of baffles and other roughness (configuration #4) elements causes a drop in the mean value of the u- component. Based on mean value measurements, we conclude that, introducing small spires results in lower mean value for u- component. The addition of conventional roughness and baffles has a similar effect on the mean flow. The wind tunnel speed presented in table 3.1 shows that the model Reynolds number is one to two orders of magnitude smaller than the full scale Reynolds number. Because the model Reynolds number is smaller than the full scale Reynolds number, the range of turbulence scales contained in the wind tunnel flow is smaller than the corresponding range at full scale. This is actually the argument for adding the roughness elements that would increase the level of turbulence and its small scale content in the wind tunnel.

3.2 Turbulence Parameters

A simple parameter that characterizes, in a global manner, the turbulence level is the turbulence intensity of the velocity components, defined as:

$$I_u = \{\frac{1}{N-1}\sum_{i=0}^{N-1} u_i^2\}^{\frac{1}{2}} / U \qquad (3.1)$$

$$I_v = \{\frac{1}{N-1}\sum_{i=0}^{N-1} v_i^2\}^{\frac{1}{2}} / U \qquad (3.2)$$

$$I_w = \{\frac{1}{N-1}\sum_{i=0}^{N-1} w_i^2\}^{\frac{1}{2}} / U \qquad (3.3)$$

Where u, v and w are fluctuating components of the longitudinal, lateral and vertical velocity components. U is the local streamwise mean velocity measured at a given height z. The turbulence intensities given by $I_{u,}$ I_v, I_w are dimensionless parameters and provide a global measure of the energy of the fluctuations relative to the mean velocity.

Comparison of I_u and I_v among all configurations, considered in this work, indicates that the different experimental setups influence both I_u and I_v . Yet, we notice some common trends. First, turbulence intensity levels of the u- component are always higher than the corresponding values of the v- component for all configurations. The addition of roughness elements, based on comparison of configurations #1 and #3, causes significant increase in both I_u and $I_{v.}$ We should note the difference between configuration #3 and #4 when baffles are added. The effects of such elements on the u- and v- components seem to go in opposite directions. While the turbulence intensity level of the u- component, $I_{u,}$ increases, the level of the v- component, $I_{v,}$ drops. This indicates that, baffles have an effect of increasing the energy of the velocity fluctuations of the u- component while decreasing the energy of the fluctuations in the lateral direction. By comparing configuration #4 and configuration #5, one can deduce that the addition of a row of small spires causes an increase in the value of $I_{v.}$ This indicates that the conventional roughness configuration , #6, and the baffle configuration #4 have some characters in common but that the conventional roughness configuration causes less velocity fluctuation. When #7 spires were added to configuration #6 to form configuration #7, the value of I_v increases much more than I_u. So the effect of such spires is clearly to increase the fluctuations in the lateral direction. Prior to 1990, most wind tunnel simulations focused on duplicating only longitudinal turbulence intensity. Recent experimental studies strongly suggest that turbulence intensity of lateral component is as important [Tieleman (1994)]. Tieleman proposed the use of #7 spires to increase the fluctuations in lateral direction in wind tunnel, which is verified by these results.

Based on the above analysis, it is concluded that small spires generate high turbulence intensity. The #7 spires produce more velocity fluctuations in the lateral direction. The baffle configuration generates more fluctuations both longitudinally and laterally as compared with the conventional configuration, #6. Among all configurations shown in table 3.1, configurations #4, #5 and #8 have the highest value of I_u. However, configurations #3, #5, #7 and #8 have the highest value of $I_{v.}$ The lowest values of both I_u and I_v component are in bare tunnel. At the same time, the biggest difference between I_u and I_v occur in configurations #4 and #6, while the smallest difference is in configuration #7. Configuration #8 has the highest turbulence intensity for both u- and v- components.

Dryden [1930] and other researchers proposed that the structure of turbulence presented in a wind-tunnel can not be adequately described by specifying the magnitude of fluctuations of the velocity components alone. It is also necessary to specify a characteristic length which is a measure of the magnitude of turbulent eddies, i.e., of the scale of the turbulence. The integral scale has been used as a measure of the largest correlation distance (time), and is defined as:

$$L_{uu} = \int_0^\infty R(\tau) d\tau \cdot U = T_{uu} \cdot U \qquad (3.4)$$

Where T_{uu} is integral time scale, U is mean velocity and L_{uu} is the integral length scale. In practical calculations, the integral presented in Equation 3.4 needs to be carried up to the point where $R(\tau)$ becomes zero. In the same manner, one can define lateral and vertical integral length scales. Table 3.1 shows that the integral length scale can be varied by having different wind tunnel configurations. Comparison of configurations #2 to #3 shows that the addition of small spires causes the value of L_{uu} to decrease from 0.76m to

0.48m. In a similar manner, the addition of smaill spires to configuration #4 as in configuration #5 causes, L_{uu} to change from 0.69 to 0.59m. L_{vv} is always smaller than L_{uu} in all configurations. However, the changing trend is the same as $L_{uu.}$ From configurations #6 to #7, changed by an additional row of #7 spires, values of both L_{uu} and L_{vv} decrease. By comparing the baffle roughness configuration and the conventional roughness configuration, the conventional roughness configuration shows lower values for both L_{uu} and L_{vv}. Among all configurations, configuration #7 has the lowest values for both L_{uu} and L_{vv}, and configurations #8 and #6 have similar values for integral length scales.

The above analysis indicates that, the influence of introducing small spires is to decrease mean velocity of u- component, increase I_u and $I_{v,}$ and decrease L_{uu}. The influence of introducing #7 spires is to decrease mean velocity of u- component, increase turbulence intensity for both directions (especially for lateral component) and decrease integral length scale. Between the baffle configuration and the conventional configuration, the baffle roughness tends to generate a flow with a lower mean velocity longitudinally, higher turbulence intensity and higher integral length scale.

3.3 Turbulence Characteristics – Fourier Domain

The above parameters provide a global measure of the effects of the different turbulence scales contained in the flow. Another measure of the level of energy in these scales can be obtained from the power spectrum. The spectrum gives the distribution of the energy among frequency components contained in the flow.

Figures 3.1 to 3.8 are plots of normalized spectral density of both u- and v- components in all wind tunnel configurations. The plots also show the theoretical blunt model proposed by Tieleman [1995] for the purpose of comparison. The plots are based on the average of 87 blocks of data, each containing 8192 measurements sampled at 4000 Hz. This provides a frequency range between 0.0305 to 2000Hz. The energy is non dimensionalized by the frequency and the variance, and the frequency is non dimensionalized by U/z, where U is the mean velocity and z is 0.0792m which corresponds to the height of the model.

In the bare tunnel, the spectra presented in figure 3.1 shows that the energy containing frequencies are higher for the v- component than for the u- component. Most of the energy in u- component is distributed between 1.5 to 4.8Hz, while most of the energy in v- component is distributed between 15 to 150Hz.

Spectra of both u- and v- components in configuration #2 presented in figure 3.2 show the variations from spectra measured for configuration #1. Frequencies with the highest energy are around 1.6Hz for both components. Thus, adding big spires to bare tunnel causes a shift of energy from the high frequencies to smaller ones. This shift must be a function of the dimensions of the big spires. It is also noted that the spectra of both the u- and v- components in configuration #2 match the blunt model better than the bare tunnel, especially at the low and intermediate frequency components.

Figure 3.3 shows the spectra of the u- and v- components in configuration #3. By comparison with the results from configuration #2 (figure 3.2), it is noted that adding the small spires causes an increase in the energy of small eddies (high frequencies) in both u- and v- components. As for low-frequencies, energy content is about the same as in configuration #2. Thus, adding small spires causes an increase in the energy of the high-

frequency components. We also noticed a better match with the blunt model than configuration #2.

Figure 3.4 shows the spectra of the u- and v- components in configuration #4. The results show perfect match of both the u- and v- component to the blunt model except for very large frequencies. Most of the energy is distributed among frequencies around 1.7Hz for both u- and v- components. Therefore, the baffle configuration generates turbulence with the bulk of its energy distributed at relatively low frequencies of the u- component, and having relatively higher energy levels at in higher frequencies for the v- component.

Spectra of the u- and v- components in configuration #5 are shown in figure 3.5. The results show a good match with the blunt model for frequencies up to 104 Hz, especially for v- component. Comparison between configurations #5 and #4 shows that small scale eddies contain more energy in configuration #5 than in configuration #4. There is no noticeable difference of the energy distribution among large scales between these two configurations, but there is a difference in the energy of the intermediate scales, which decreases slightly when small spires are added. The change occurring from configuration #4 to configuration #5 is in agreement with the results deduced from the comparison of configurations #2 and #3 with respect to the effect of adding small spires to the wind tunnel.

The spectra of the u- and v- components in configuration #6 are shown in figure 3.6. Both u- and v- spectra match the blunt model very well for large and intermediate scales. Shapes of the spectra are closer to those of configuration #5 than configuration #4. The highest energy distribution occurs at about 1.4Hz for u- and 7.7Hz for v- component.

The spectra of the u- and v- components in configuration #7 are shown in figure 3.7. In comparison with configuration #6, the energy is shifted from large scales to smaller

scales for both u- and v- components. Thus the #7 spires enhance the level of energy of the high frequency components.

Configuration #8 has a radically different configuration system when compared with the previous ones. Its u- and v- spectra, shown in figure 3.8, are close to those of configuration #3 which is the bare tunnel plus big and small spires. The highest energy distribution in configuration #8 is around 1.6Hz. The overall distribution of energy among frequencies of configuration #8 is similar to that in configuration #5.

The above spectral analysis indicates that, the influence of introducing small spires to the energy distribution is to decrease energy distribution among frequencies between 1 to 11 Hz, while increasing the distribution for the higher frequencies. The energy level in the large scales does not vary much. Small spires cause also a shift of energy from intermediate scales to smaller scales. Difference between configurations #6 and #7 shows that the effect of adding #7 spires is to shift energy from large scales to small scales for u-component. For the v- component, energy distribution in large scales decreased drastically, while energy of the small scales does not increase much. Comparison of configurations #4 and #6 indicates there is no significant difference of energy distribution, indicating these configurations have a similar effect with respect to spectral simulation.

3.4 Small Scale Turbulence

The generation of small-scale fluctuations in turbulence is due to non-linear activity, however viscosity prevents the generation of infinite small scales of motion by dissipating small-scale energy into heat. The magnitude of small scales in table 3.1 is calculated according to the following equation [Melbourne, (1980)].

$$S = \frac{\sigma_u^2}{U^2} \cdot \frac{n S_u(n)}{\sigma_u^2} \Bigg|_{\frac{U}{n} \approx \frac{L}{10}} \qquad (3.5)$$

Where the $S_u(n)$ is the power spectra of velocity component, U is the mean velocity of the u- component, σ_u^2 is the variance, and L is the characteristic dimension of the model. For a low-rise model, where the height of the model is less than the plane dimension, L takes the value of H [Tieleman, (1996)].

Among all flows, those of configurations #5, #7 and #3 have the highest S values. Configurations #1 and #2 have the lowest S values. It is obvious that, introducing small spires causes an increase in the value of S. By adding small spires to configuration #2, S_u changes from 1.05×10^{-7} to 3.86×10^{-7}. By adding small spires to configuration #4, the value of S increases from 2.86×10^{-7} to 6.40×10^{-7}. The effect of configuration #7 spires also increases the energy level of the small scales as indicated by a change of S_u from 2.05×10^{-7} to 5.46×10^{-7} from configurations #6 to #7. The addition of baffles also causes an increase in the value of S, based on comparison with conventional roughness configuration, although the difference is not big. Values of S for configuration #8 are in between the values for the base configuration and base configuration plus small spires. The base configuration refers to baffle and conventional roughness configurations, #4, #6 respectively. Therefore, introducing small spires increases small-scale parameter S. The introduction of #7 spires also causes an increase of this parameter. Between the baffle configuration and the conventional configuration, baffle roughness tends to generate a higher small-scale parameter S.

In this chapter we have shown how time and frequency domain parameters characterize the simulated turbulence in different configurations. However, one problem with these parameters is that they do not provide a measure of time variations of energy levels. Therefore, they could not be related to negative pressure peaks observed over much smaller time lengths. This limitation is due to the fact that many of the parameters presented in this chapter are averaged over long periods in order to have stable estimates.

In next chapter, we will see how parameters obtained via wavelet analysis can help in solving this problem.

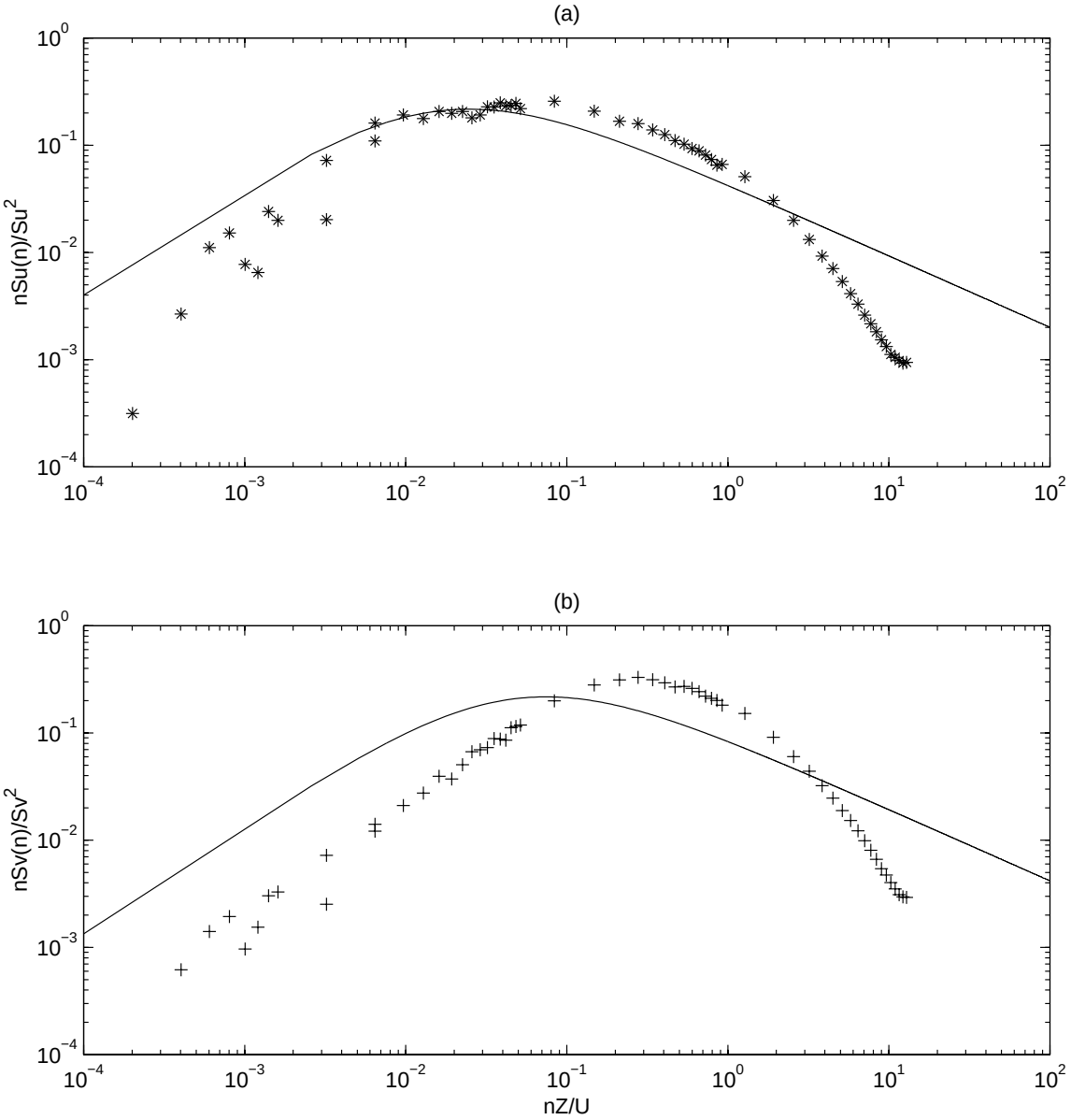

Figure 3.1 Power spectra of velocity components of configuration #1 --- * and the blunt model --- —
(a) u- component (b) v- component

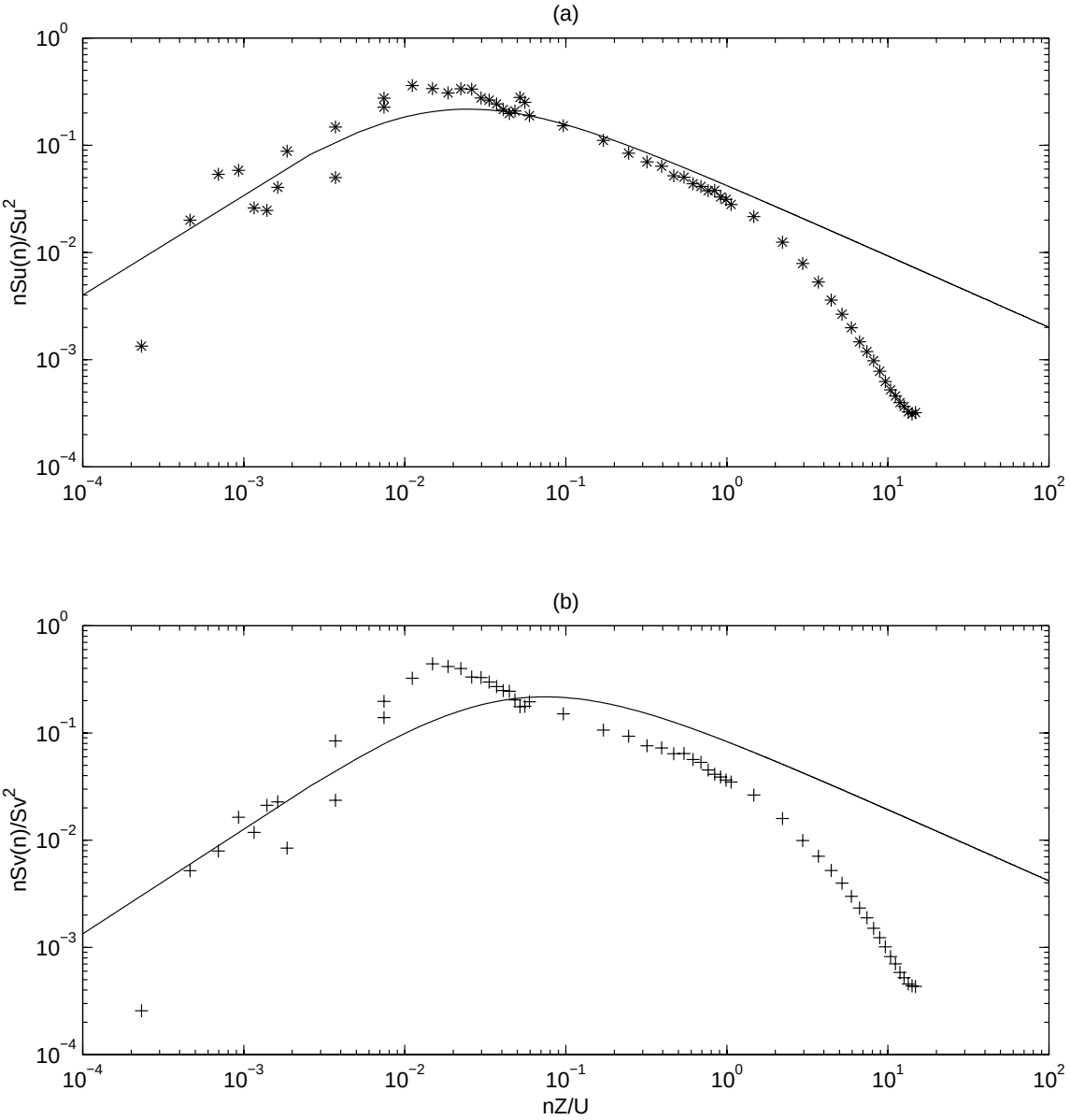

Figure 3.2 Power spectra of velocity components of configuration #2 --- * and the blunt model --- —
(a) u- component (b) v- component

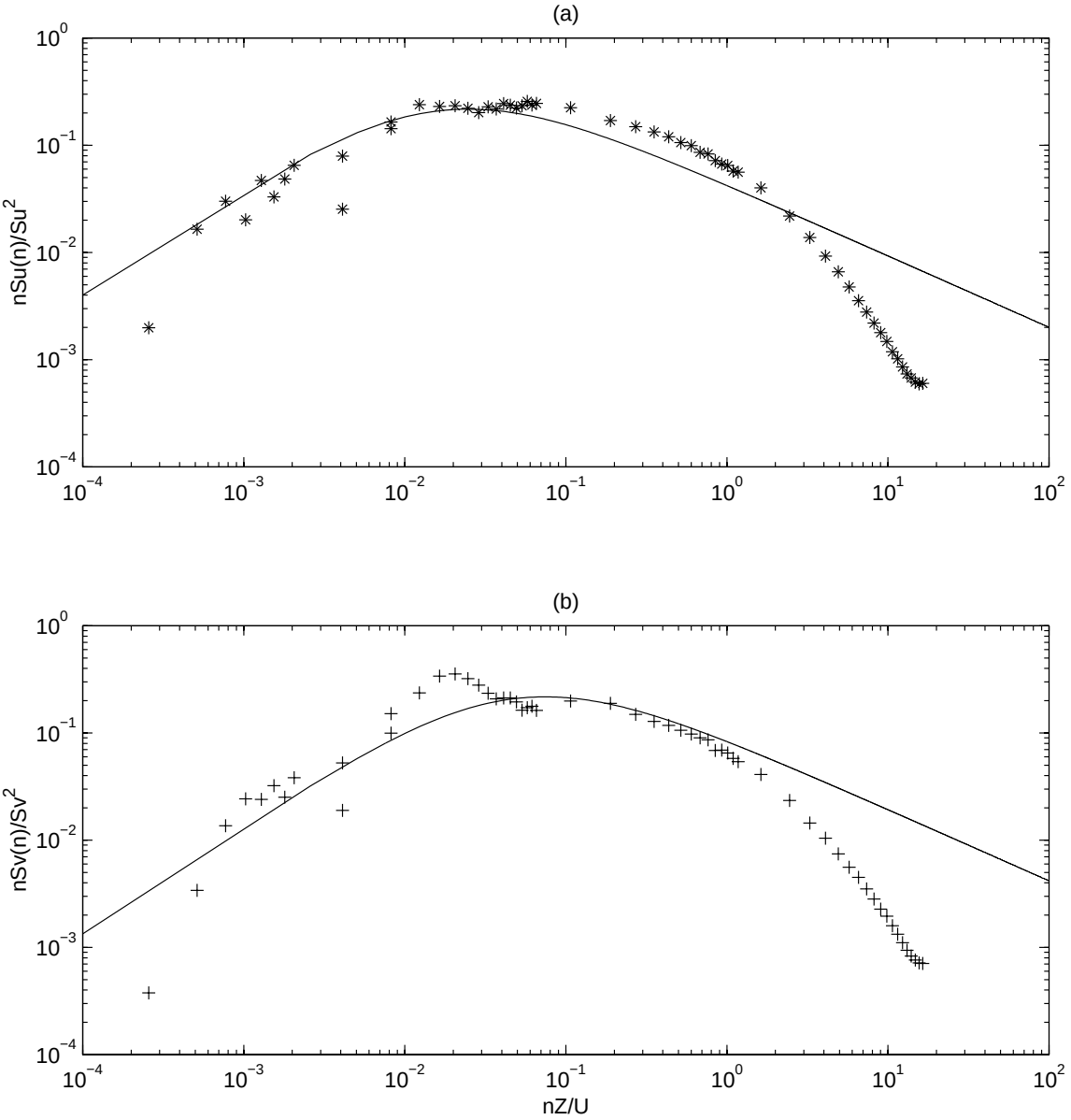

Figure 3.3 Power spectra of velocity components of configuration #3 --- * and the blunt model --- —
(a) u- component (b) v- component

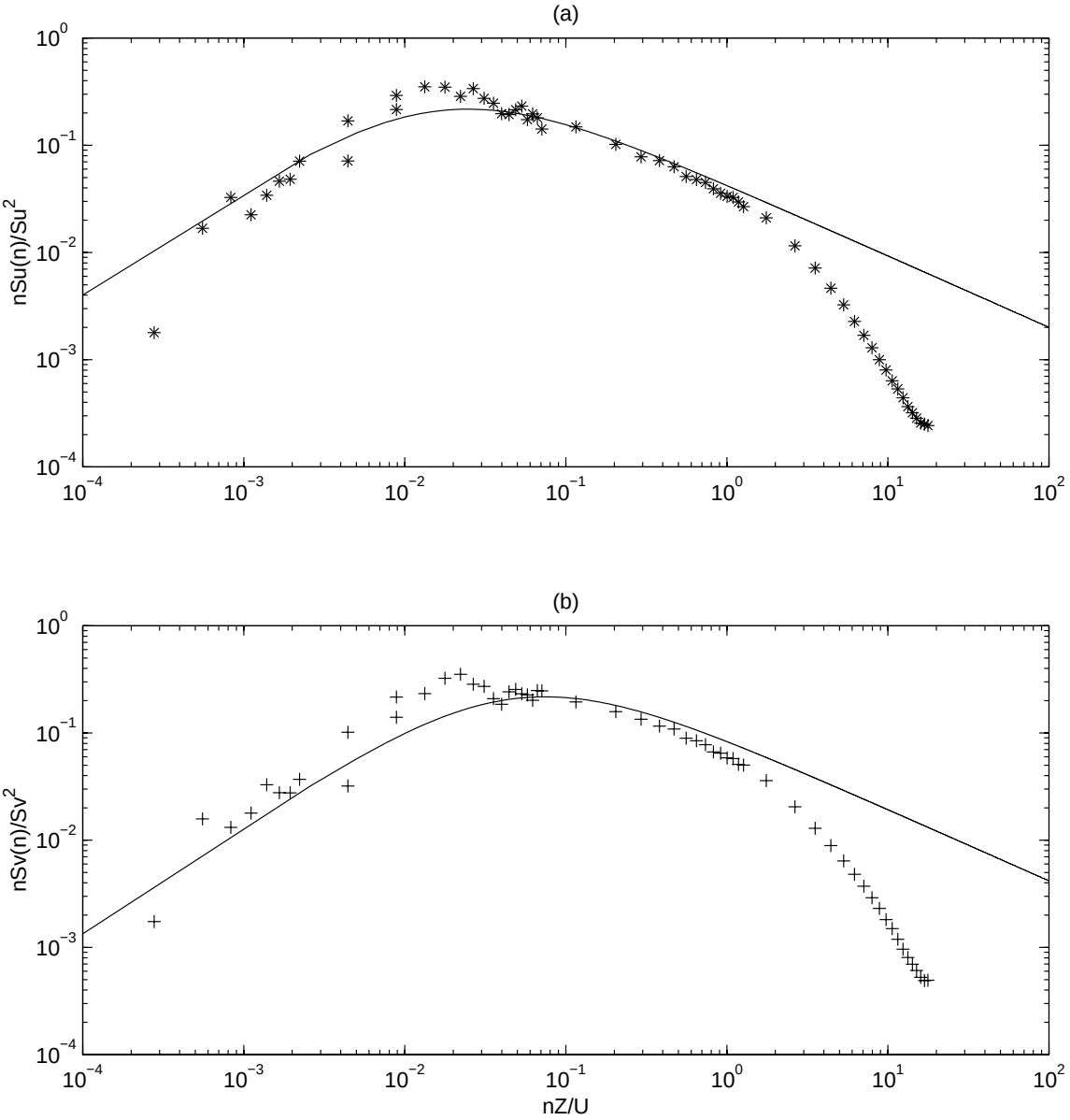

Figure 3.4 Power spectra of velocity components of configuration #4 --- * and the blunt model --- —
(a) u- component (b) v- component

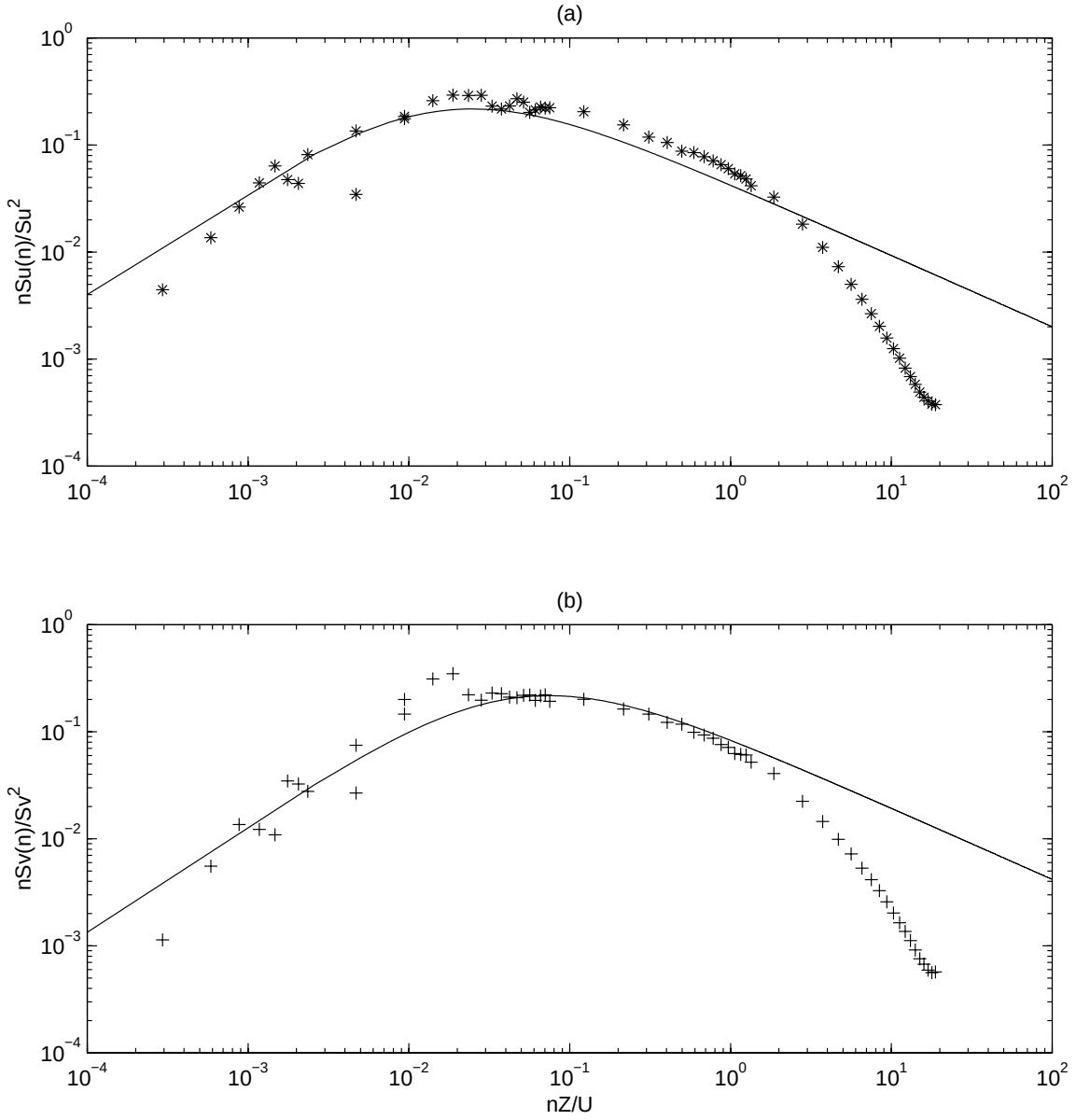

Figure 3.5 Power spectra of velocity components of configuration #5 --- * and the blunt model --- — (a) u- component (b) v- component

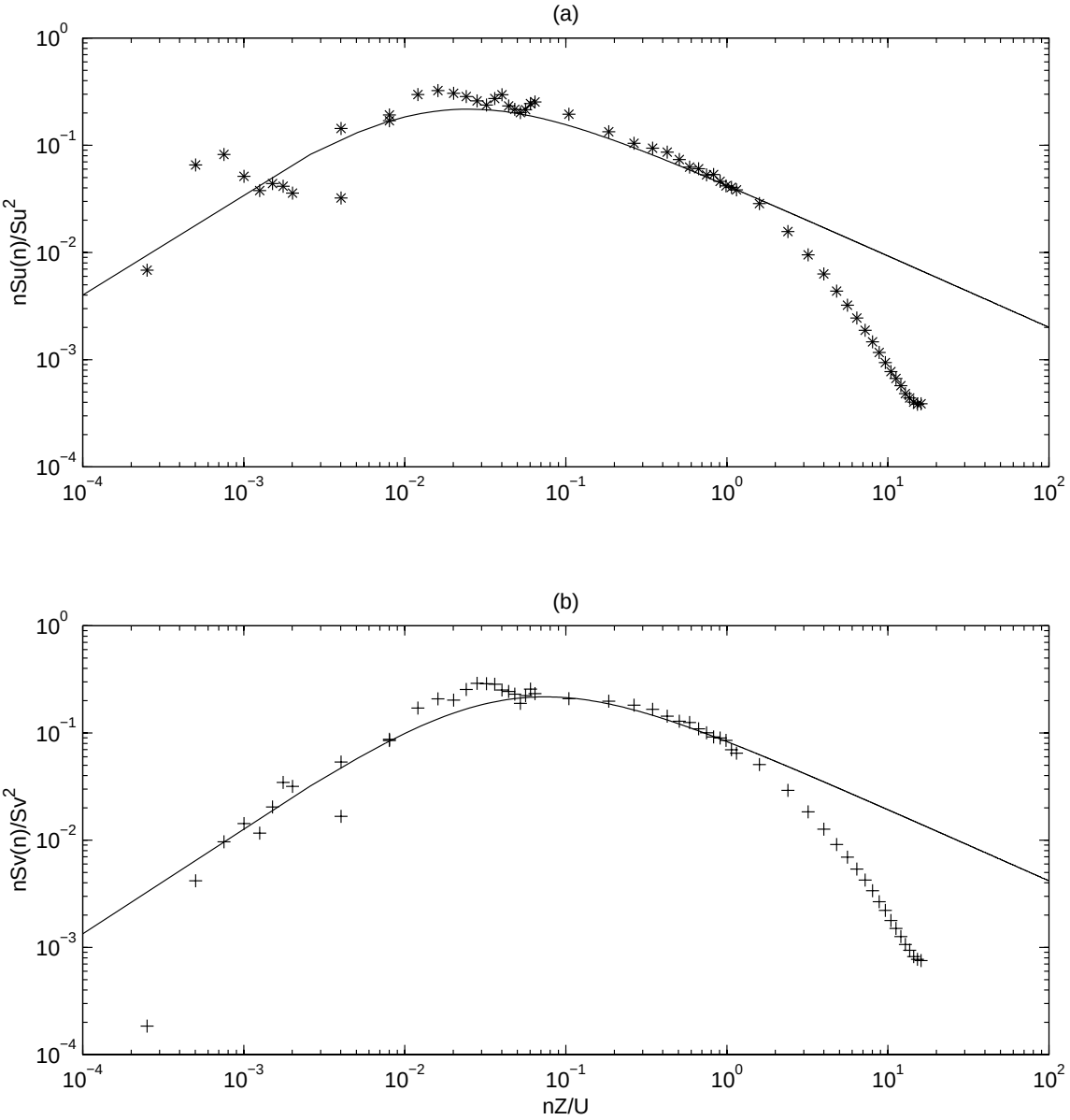

Figure 3.6 Power spectra of velocity components of configuration #6 --- * and the blunt model --- —
(a) u- component (b) v- component

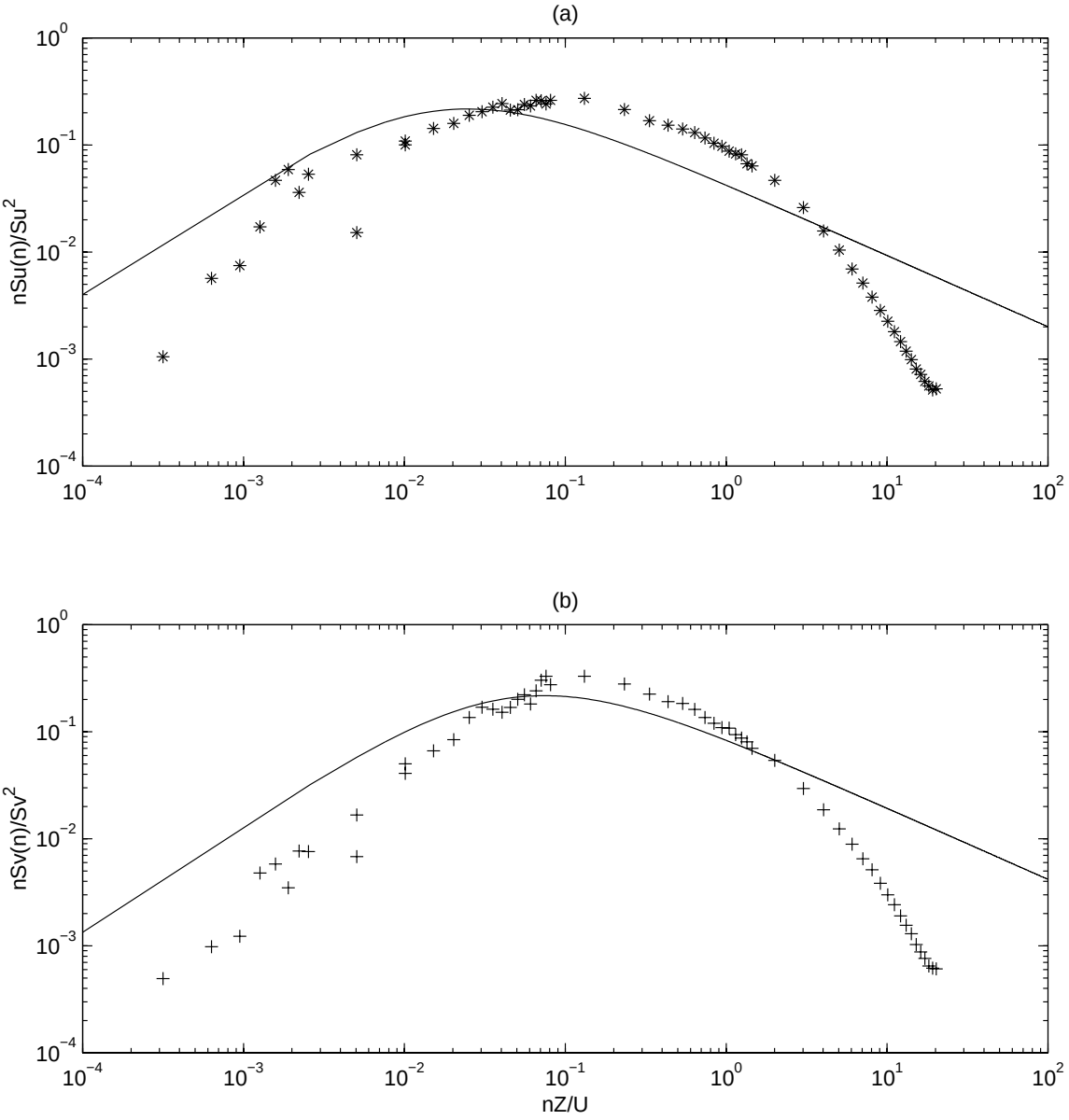

Figure 3.7 Power spectra of velocity components of configuration #7 --- * and the blunt model --- —
(a) u- component (b) v- component

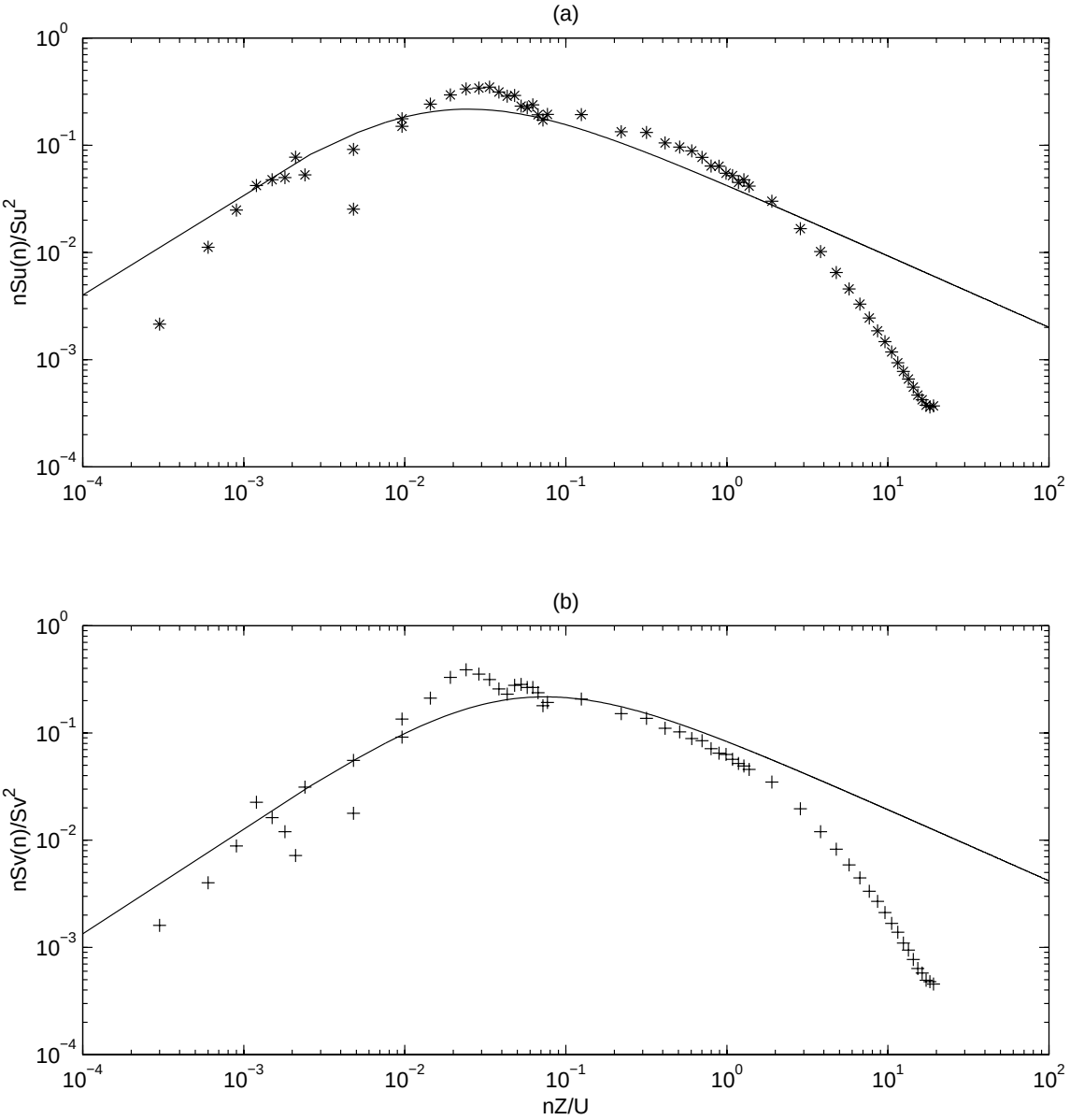

Figure 3.8 Power spectra of velocity components of configuration #8 --- * and the blunt model --- —
(a) u- component (b) v- component